World Academy of Science, Engineering and Technology
International Journal of Aerospace and Mechanical Engineering
Vol:3, No:1, 2009

Vortex Shedding at the End of Parallel-plate Thermoacoustic Stack in the Oscillatory Flow Conditions

Lei Shi, Zhibin Yu, Artur J. Jaworski, and Abdulrahman S. Abduljalil

Open Science Index, Aerospace and Mechanical Engineering Vol:3, No:1, 2009 publications.waset.org/10616.pdf

Abstract**—**This paper investigates vortex shedding processes occurring at the end of a stack of parallel plates, due to an oscillating flow induced by an acoustic standing wave within an acoustic resonator. Here, Particle Image Velocimetry (PIV) is used to quantify the vortex shedding processes within an acoustic cycle phase-by-phase, in particular during the "ejection" of the fluid out of the stack. Standard hot-wire anemometry measurement is also applied to detect the velocity fluctuations near the end of the stack. Combination of these two measurement techniques allowed a detailed analysis of the vortex shedding phenomena. The results obtained show that, as the Reynolds number varies (by varying the plate thickness and drive ratio), different flow patterns of vortex shedding are observed by the PIV measurement. On the other hand, the time-dependent hot-wire measurements allow obtaining detailed frequency spectra of the velocity signal, used for calculating characteristic Strouhal numbers. The impact of the plate thickness and the Reynolds number on the vortex shedding pattern has been discussed. Furthermore, a detailed map of the relationship between the Strouhal number and Reynolds number has been obtained and discussed.

Keywords**—**Oscillatory flow, Parallel-plate thermoacoustic stack, Strouhal numbers, Vortex shedding.

I. INTRODUCTION

OSCILLATORY flows past bluff bodies may lead to very complex flow patterns because vortices shed in one half of the oscillation cycle, on one side of the bluff body, may impinge on it when the flow reverses and may interact with vortices generated in the second half of the cycle on the other side of the bluff body. These phenomena have been a subject of many numerical and experimental studies. For example, Chung and Kang [1] and Barbi et al. [2] investigated interesting "lock-on" effects between the vortex shedding behind a cylinder and the oscillatory incoming flow using a numerical analysis. Tatsuno and Bearman [3] investigated the morphology of the flows generated by oscillating cylinders in a stationary fluid as a function of various similarity parameters, while similar studies were performed by Okajima et al. [4] for square cylinders, to name but a few.

It should be noted that somewhat related flow phenomena, including vortex shedding, also arise in thermoacoustic systems (engines or refrigerators) where high amplitude acoustic excitation leads to oscillatory flows past the internal structures responsible for the heat transfer mechanisms associated with the so called "thermoacoustic effect", see for example Swift [5], [6]. These structures often include stacks, regenerators and heat exchangers, which in the simplest case may take the form of stacks of parallel plates. Due to the geometrical discontinuities of the stack and the oscillatory nature of the flow induced by the high-intensity acoustic field, the flow phenomena at the end of the stack plates are very complex and largely dominated by concentrated vortices shed from the plate ends, and their subsequent dissipation into turbulence. These processes greatly affect the energy transfer and thus the performance of the thermoacoustic devices. Therefore, further development of thermoacoustic devices requires their detailed understanding, which is the motivation behind the current work.

Experimental studies of the above phenomena within the thermoacoustic systems are relatively limited. Blanc-Benon et al. [7] investigated the flow structures shed from a stack of parallel plates at relatively low drive ratios of between 1.0 and 1.5% using Particle Image Velocimetry (PIV) and compared the results with numerical simulations. Here, the drive ratio (Dr), is usually used to characterize the intensity of the acoustic standing wave, and is defined as the ratio of the peak pressure amplitude to the mean pressure. They used two configurations of stacks ("thin" and "thick" plates) to reveal "elongated" and "concentrated" symmetrical vortices, but never fully detached from the plates. Mao et al. [8] conducted further PIV studies to show the processes of vortex evolution at higher drive ratios (up to 2%), using two stacks with 1 and 5 mm thick plates, and with fixed spacing between the plates (5 and 10 mm, respectively).

The present paper is an extension of previous work described in Mao et al. [8] in that it investigates a wider parameter range (the plate thickness: 0.5, 1, 1.5, 2, 3, 4 and 5 mm, and plate spacing between 1.2 and 10.8 mm) and tries to cover more systematically the Reynolds number range up to 5,000. The

L. Shi, Z. Yu and A. S. Abduljalil are with the School of Mechanical, Aerospace and Civil Engineering, the University of Manchester, Sackville Street, PO Box 88, Manchester M60 1QD, UK. (Their e-mails are: Lei.Shi@postgrad.manchester.ac.uk, Zhibin.Yu@manchester.ac.uk and aalsayed@gmail.com, respectively).

A. J. Jaworski, the corresponding author, is with the School of Mechanical, Aerospace and Civil Engineering, the University of Manchester, Sackville Street, PO Box 88, Manchester M60 1QD, UK.(Tel: +44(0)1612754352; fax: +44(0)8701307474; e-mail: a.jaworski@manchester.ac.uk).

relationship between the Reynolds number and the Strouhal number related to vortex shedding frequency is investigated further.

II. EXPERIMENTAL SETUP AND METHOD

The experimental rig used is shown schematically in Fig. 1. The 7.4 meters long resonator is a metal tube with a square internal cross section of 134mm x 134mm. It is joined with a cube-shaped loudspeaker box, on which one 18 inches diameter, 600 W loudspeaker, Model PD1850, is mounted to generate an acoustic standing wave within the resonator. The acoustic coupling between the resonator and the loudspeaker generates a quarter-wavelength acoustic wave with the fundamental frequency 13.1 Hz. The resonator is filled with air at atmospheric pressure and at room temperature. The resonator is equipped with a piezoresistive pressure transducer (Endevco Model 8510B-2) to measure the pressure amplitude at one end of the resonator, which is used as a reference signal to trigger PIV measurements, phase locked to the acoustic cycle.

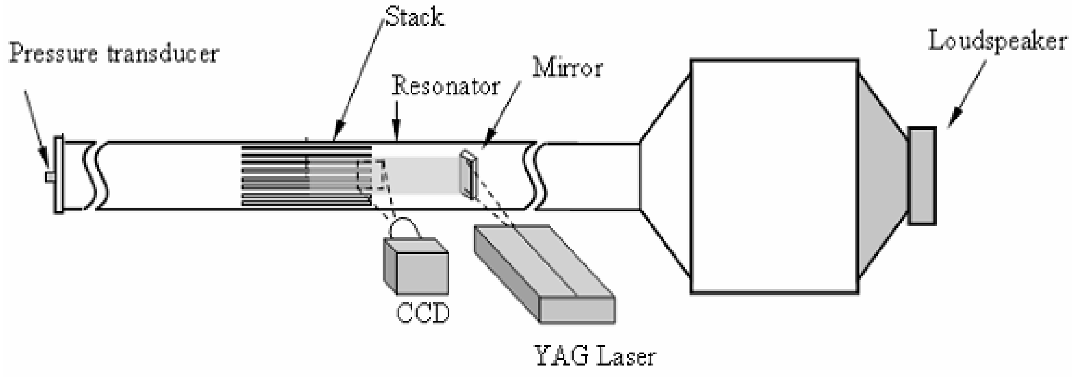

Fig. 1 Sketch of the experimental apparatus

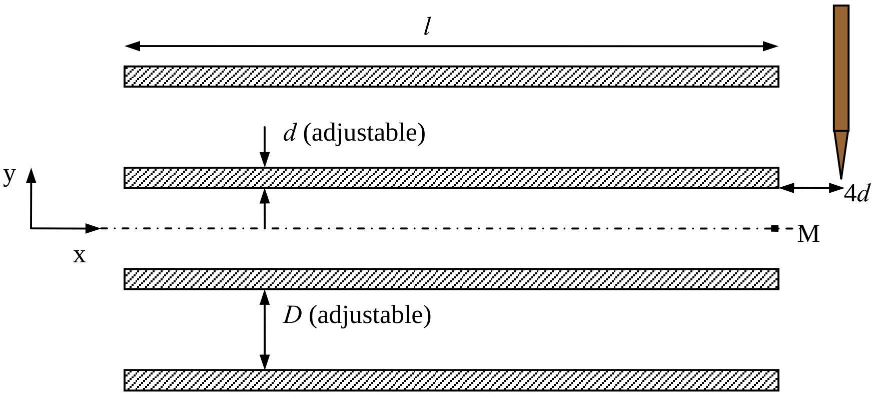

Fig. 2 Geometry of the stack (only four plates shown)

The experiments were conducted for a series of stacks, which are shown schematically in Fig. 2. The length, l, of all the stacks is 200mm, while their width is 132mm. There are seven different sizes of stack, whose plates are 0.5, 1, 1.5, 2, 3, 4 and 5 mm in thickness (d), respectively. Each stack is tested for three values of plate spacing (D), which varies from 1.2mm to 10.8mm. Table I summarizes the stack geometrical dimensions and flow conditions used in this work. The table contains porosity, Φ, defined as the cross sectional area of the stack occupied by air over the cross-sectional area of the resonator. For a stack of evenly spaced plates, this can be approximated by $D/(D+d)$. For a given stack geometry the flow velocity amplitude and the corresponding Reynolds number can be controlled by varying the drive ratio. The Reynolds number, Re_d, is defined as

$$\mathrm{Re}_d = u_M d / \upsilon , \qquad (1)$$

where υ is the kinematic viscosity of air at ambient conditions, u_M is the velocity amplitude at point M in Fig. 2. The stack is placed in the resonator 4.6 meters (about 0.17 of the wavelength) from the end cap of the resonator.

Flow field measurements were performed using a PIV system by LaVision. The laser sheet is generated by a dual Nd:YAG laser with a wavelength of 532nm, and combined with sheet optics and divergence lens. It enters the resonator perpendicularly to its axis, is reflected by a small mirror and becomes parallel to the resonator axis and normal to the surface of the stack plates. Images are taken by LaVision Imager Pro plus camera with a 4 mega-pixel CCD sensor and post processed using commercial software LaVision DaVis 7.2. The flow is seeded with olive oil droplets, produced by an oil droplet generator (TSI's model 9307). The mean droplet diameter is 1 micron. Cross correlation mode is used and the interrogation window is 16 pixels by 16 pixels. The field of view of the PIV images varied from 15 mm × 15 mm to 60 mm × 60 mm, depending on the flow features to be imaged. The maximum spatial resolution was 0.12 mm.

Flow field measurements were performed at 20 phases in one acoustic cycle as illustrated in Fig. 3. A phase locked circuit was developed and combined with TTL signal generator to trigger the laser action and record the image by the camera. For each phase, 100 pairs of frames were taken to calculate the phase-averaged velocity vector fields. Here, two flow stages are defined according to fluid flow direction. In Fig. 2, when the velocity at point M is toward the positive direction of x coordinate (corresponding to phases ϕ_1 through to ϕ_{10} as illustrated in Fig. 3), it is referred to as an "ejection" stage; whereas when it is toward the negative direction of x coordinate (corresponding to phases ϕ_{11} through to ϕ_{20}), it is referred to as a "suction" stage. For convenience of further explanation the ejection stage can be further subdivided into acceleration and deceleration stages: $\phi_1 - \phi_5$ and $\phi_6 - \phi_{10}$, respectively.

For further investigation of vortex shedding frequencies, a standard hot-wire anemometry system, TSI IFA300, was used to detect velocity fluctuations near the end of the stacks. As shown in Fig. 2, the hot-wire probe is normal to the plate and the axis of the resonator, and is placed 4*d* from the edge of the plate. The hot-wire signals were recorded with a sampling frequency of 5000 Hz.

TABLE I

SUMMARY OF STACK DIMENSIONS AND EXPERIMENTAL CONDITIONS

d(mm)	D(mm)	Φ	Dr(%)	u_M(m/s)	Re_d
0.5	1.2	0.70	1.5	6.14	207
0.5	1.2	0.70	2.0	8.37	281
0.5	2.4	0.82	2.0	7.32	246
0.5	2.4	0.82	3.0	10.61	357
0.5	4.8	0.90	3.0	9.39	316
1	2.4	0.71	1.0	4.31	281
1	2.4	0.71	1.5	6.23	407
1	2.4	0.71	2.0	8.53	557
1	2.4	0.71	3.0	12.28	801
1	4.8	0.83	1.5	4.95	323
1	4.8	0.83	2.0	6.63	433
1	4.8	0.83	3.0	10.39	678
1	7.2	0.88	2.0	5.92	386
1	7.2	0.88	3.0	9.42	614
1.5	6.0	0.80	1.0	5.20	518
1.5	6.0	0.80	1.5	6.94	691
1.5	6.0	0.80	2.0	8.67	863
1.5	6.0	0.80	3.0	10.41	1036
2	6.0	0.73	1.5	5.35	780
2	6.0	0.73	2.0	7.41	1079
2	6.0	0.73	3.0	11.43	1665
2	8.4	0.79	1.5	4.85	706
2	8.4	0.79	2.0	6.62	965
2	8.4	0.79	3.0	10.39	1513
3	6.0	0.67	3.0	12.76	2523
3	8.4	0.74	1.5	5.19	1026
3	8.4	0.74	2.0	7.15	1414
3	8.4	0.74	3.0	10.96	2167
4	4.8	0.54	1.5	6.95	1859
4	4.8	0.54	2.0	9.40	2514
4	7.2	0.64	1.0	4.09	1095
4	7.2	0.64	1.5	6.24	1671
4	7.2	0.64	2.0	8.49	2273
4	7.2	0.64	3.0	12.79	3424
4	9.6	0.70	1.5	5.21	1395
4	9.6	0.70	2.0	7.11	1904
4	9.6	0.70	3.0	11.08	2965
5	10.0	0.66	2.0	6.20	2045
5	10.0	0.66	3.0	9.54	3144
5	10.8	0.68	2.0	13.36	4508
5	10.8	0.68	3.0	12.09	4081

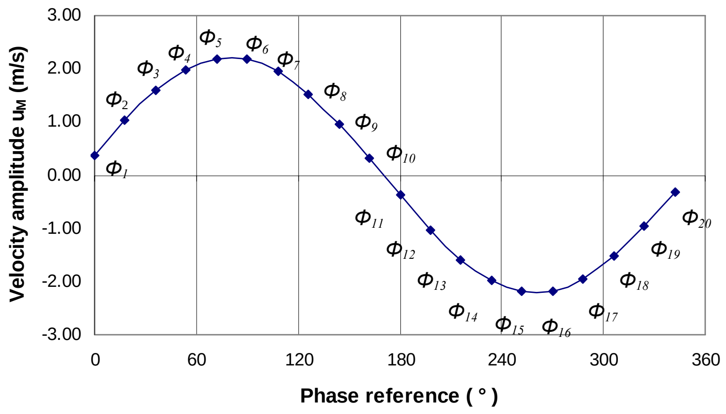

Fig. 3 Phase-averaged velocity at point M and 20 tested phases (d = 1mm, D = 4.8mm, Re_d = 123, Dr = 0.6%).

III. EXPERIMENTAL RESULTS

A. PIV Experimental Results

Vortex shedding processes at the end of the stack in the oscillatory flow have been visualized by Mao et al. [8] and Berson et al. [9]. Both of them found that shedding vortices appear in the ejection stage. At small Reynolds numbers (corresponding to low acoustic amplitudes) attached symmetric vortices are generated. When the Reynolds number is increased, the flow patterns characterised by attached vortices turn into flow patterns exhibiting clear vortex shedding processes (where discrete vortices detach from the edges of the stack plates). This paper presents vortex shedding pattern using PIV for more stack sizes as shown in Table I.

Figures 4-6 show three typical cases of the vortex shedding patterns obtained using PIV near the end of the stack. As the vortex shedding flow phenomena mainly occur in the ejection stage as explained above, only six most characteristic phases ($\phi_2, \phi_4, \phi_5, \phi_7, \phi_8, \phi_{10}$) are presented. The details of the selected flow patterns are described below.

Figure 4 presents the vorticity field for the stack with plate thickness d = 0.5 mm and plate spacing D = 4.8 mm, for Re_d = 207 and Dr = 2.0%. At the beginning of the ejection stage, as shown in Fig. 4a (ϕ_2), the flow starts to accelerate and forms a pair of attached vortex structures at the end of the plate. They are symmetrical relative to the centre-line of the plate. As the velocity gradually increases the flow pattern changes accordingly. The attached vortex structures become more elongated but still remain symmetrical as can be seen in Figs. 4b (ϕ_4) and 4c (ϕ_5). When the flow velocity nearly reaches its peak, the elongated vortex structures start to become unstable – see the bottom "wake" in Fig. 4c (ϕ_5). As the flow enters the deceleration stage, the elongated vortex structures break up into a series of more discrete vortices which can be likened to a classical "vortex street", as illustrated in Figs. 4d and 4e (ϕ_7 and ϕ_8, respectively). This could be explained by the fact that oscillatory flows become generally more unstable in the deceleration stage [10]. At the end of the deceleration stage – see Fig. 4f (ϕ_{10}) – the flow slows down and the elongated "vortex street" gradually disappears. Finally, the flow reverses during the suction stage of the cycle.

Figure 5 gives the vorticity fields for d = 1 mm, D = 4.8 mm, Re_d = 433 and Dr = 2.0%. As before, only six selected phases are shown. The main difference compared to the structures discussed with reference to Fig. 4 is that the attached symmetrical vortex structures in Fig. 5b (ϕ_4) are no longer elongated, but begin to break up early and into discrete vortices, which look as though they were shed alternately from the top and the bottom side of each plate. As the flow velocity increases further in Fig. 5c (ϕ_5), this vortex shedding pattern extends very far from the plate. Some discrete vortex structures far from the plates merge with one another when the flow starts to decelerate – as seen in Fig. 5d (ϕ_7). As flow velocity decreases further, the vortex shedding wakes become relatively short – see Fig. 5e (ϕ_8).

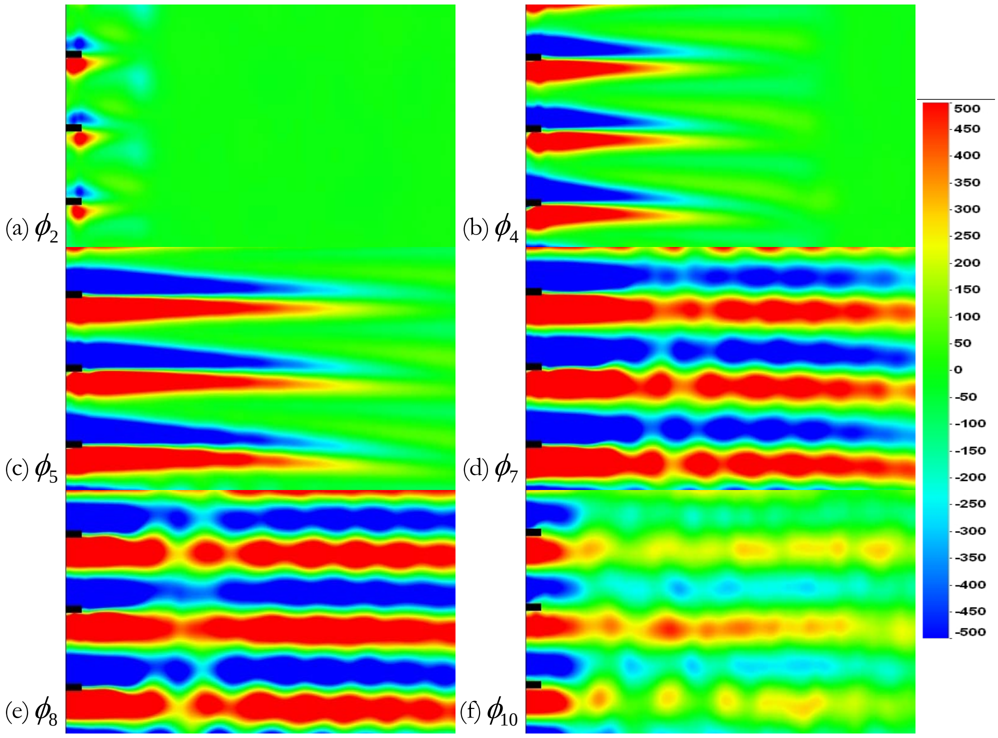

Fig. 4 Vorticity fields for the flow at the end of stack (d = 0.5mm, D = 4.8mm, Re_d = 207, Dr = 2.0%). The unit of vorticity legend is s^{-1}

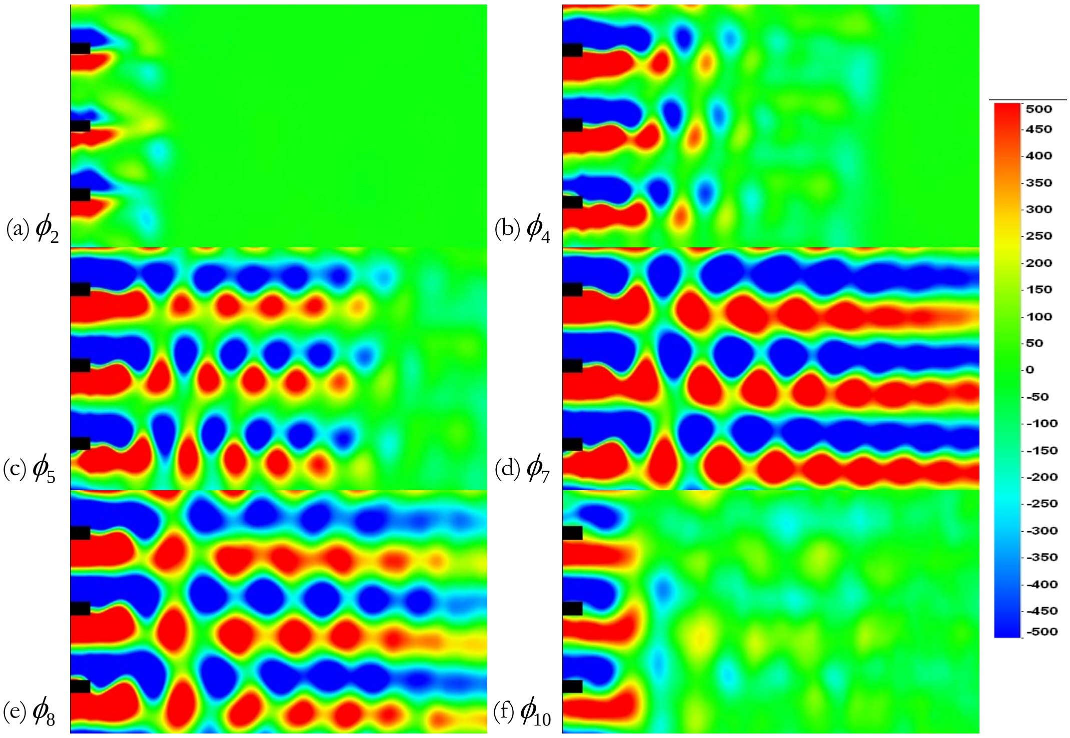

Fig. 5 Vorticity fields for the flow at the end of stack (d = 1mm, D = 4.8mm, Re_d = 433, Dr = 2.0%). The unit of vorticity legend is s^{-1}

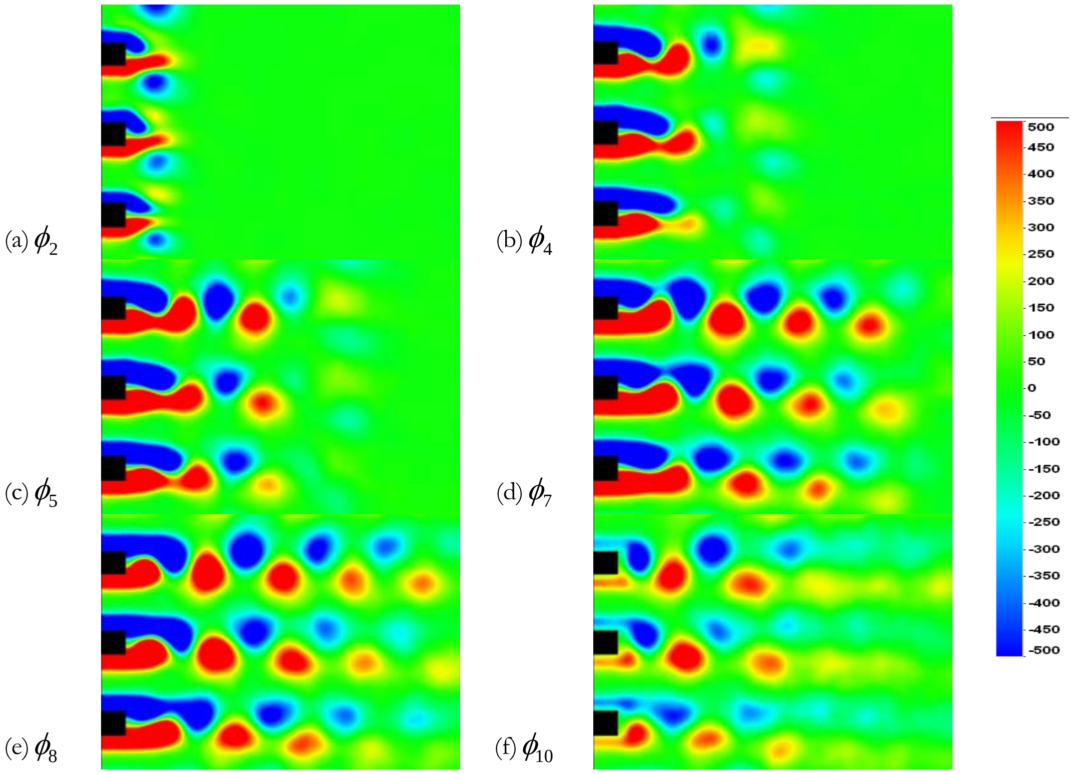

Fig. 6 Vorticity fields for the flow at the end of stack (d = 4mm, D = 9.6mm, Re_d = 1395, Dr = 1.5%). The unit of vorticity legend is s^{-1}

Vorticity fields for d = 4 mm, D = 9.6 mm, Re_d = 1395 and Dr = 1.5% are shown in Fig. 6. Compared to the previous two cases described with reference to Figs. 4 and 5, it is clear that the dominating mechanism for the appearance of the "vortex street" is alternate shedding at the end of the plate, rather than a break up of unstable elongated shear layers (see Fig. 6c). This flow pattern of the alternate vortex shedding dominates for the whole deceleration stage, and can still be seen in Fig. 6f (ϕ_{10}).

B. Hot-wire Anemometry Results

In order to obtain further insight into the various vortex shedding phenomena described in section 3.1, hot-wire anemometry is used to measure the unsteady flow velocity signals behind the end of a selected plate in the stack. Of course, the hot-wire measurement has a higher temporal resolution than PIV and hence it is possible to perform a full frequency analysis.

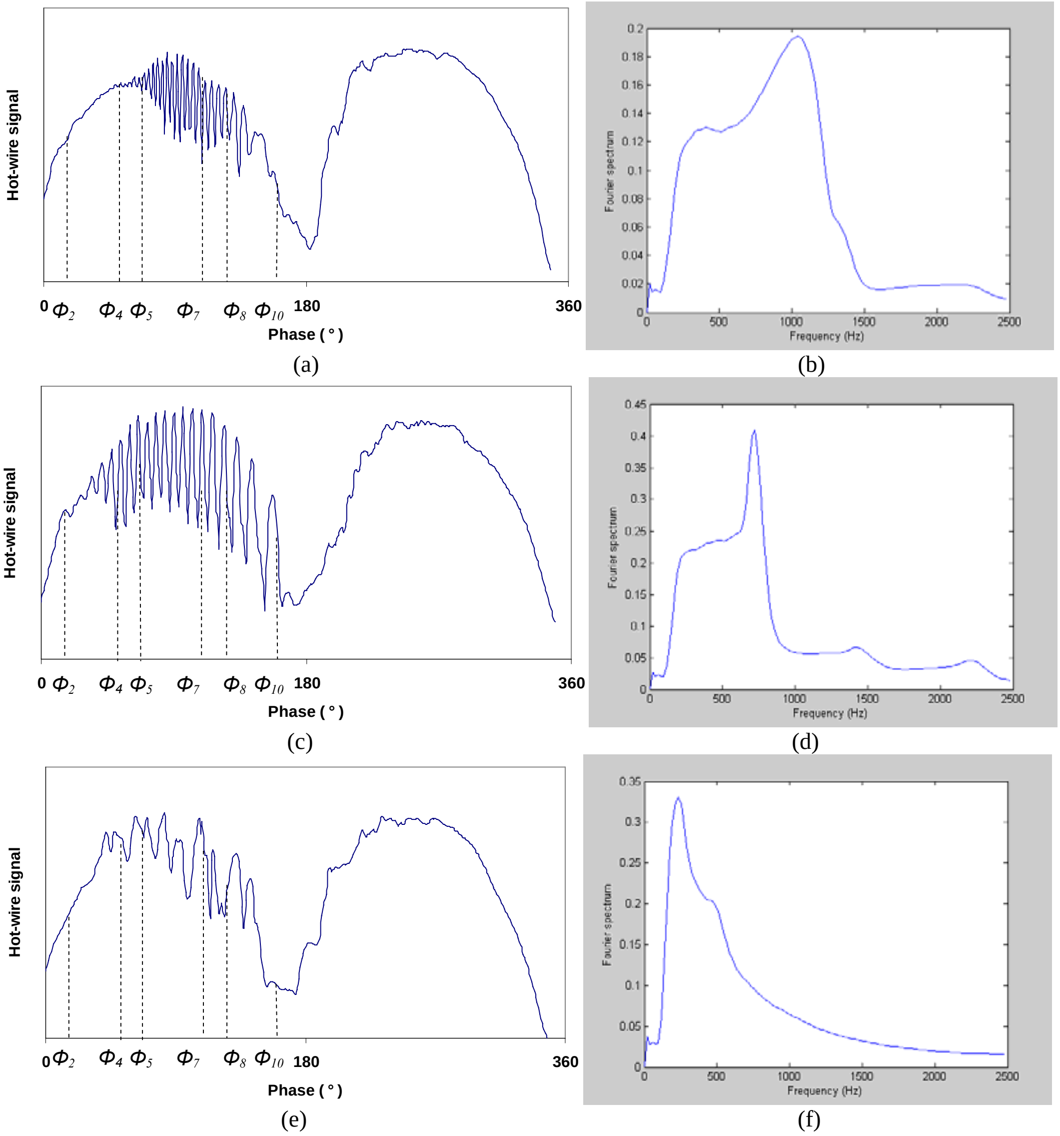

(a) (b)

(c) (d)

(e) (f)

Fig. 7 Hot-wire signal traces within an acoustic cycle and the corresponding frequency spectrum; a, b (d = 0.5mm, D = 4.8mm, Re_d = 207, Dr = 2.0%); c, d (d = 1mm, D = 4.8mm, Re_d = 433, Dr = 2.0%); e, f (d = 4mm, D = 9.6mm, Re_d = 1395, Dr = 1.5%)

The hot-wire signal traces obtained in one acoustic cycle, corresponding the three cases illustrated in Figs. 4-6 are plotted in Figs. 7a, 7c and 7e, respectively. The corresponding phases in Figs. 4-6 are also marked with dashed lines.

The fast Fourier transform (FFT) algorithm is used to estimate the vortex shedding frequency. The high order polynomial is used to filter out the low-frequency sinusoidal signal. The filtered signal traces are divided into many data windows, each containing 256 data points, starting at the same phase of the acoustic cycle, and covering the whole fluctuation burst in the “ejection” stage. For each window of data, a frequency spectrum is obtained. All such frequency spectra obtained for a given experimental run are ensemble averaged, and a mean frequency spectrum is obtained. The peak frequency of the frequency spectrum corresponds to the dominating vortex shedding frequency. Figs. 7b, 7d, 7f show the frequency spectra of the corresponding signal traces in the left column of Fig. 7. A detailed discussion of the hot-wire signal traces is given below.

Fig. 7a gives the hot-wire signal trace for d = 0.5 mm, D = 4.8 mm, Re_d =207 and Dr = 2.0%. At the beginning of the acceleration stage, the hot-wire signal shows smooth rise in profile. It is related to a pair of attached symmetric vortex structures as shown in Fig. 4a (ϕ_2). For phase ϕ_4 , still relatively smooth profile corresponds to a pair of attached elongated symmetric vortex structures in Fig. 4b. By phase ϕ_5, the signal begins to show slight fluctuations, which agrees with that the attached vortex structures are not stable and start to shed from the plates as shown in Fig. 4c. After this phase, the signal exhibits very strong fluctuations (see ϕ_7 and ϕ_8) corresponding to the break up of the elongated vortices and the emergence of the "vortex street" of more discrete vortices in Figs. 4d and 4e. After phase ϕ_8, the fluctuations of the hot-wire signal become weak, and disappear almost completely by phase ϕ_{10}. This compares well with the lack of any vortex shedding in Fig. 4f.

The hot wire signal trace for d = 1 mm, D = 4.8 mm, Re_d =433 and Dr = 2.0% are shown in Fig. 7c. At phase ϕ_2, the hot-wire signal trace exhibits a continuous and smooth change corresponding to the attached symmetric vortex structures in Fig. 5a. With the increase of velocity, the fluctuations in the hot-wire signal appear somewhat earlier compared to the previous case, namely before phase ϕ_4, which corresponds to the fact that the break up of the elongated vortices in Fig. 4 takes place later than the clear alternate shedding in Fig. 5. The fluctuation amplitude becomes more pronounced as the velocity increases further (see phase ϕ_5). When entering the deceleration stage, the strong fluctuations in the hot-wire signal persist until phase ϕ_{10}. The changes in the character and magnitude of recorded fluctuations correspond to the evolution of the vortex shedding patterns as described with reference to Fig. 5.

Fig. 7e presents the hot-wire signal trace for d = 4 mm, D = 9.6 mm, Re_d = 1395 and Dr = 1.5%. At phase ϕ_4, small fluctuations start to appear. They correspond to the beginning of the shedding processes shown in Fig. 6b. The fluctuations persist until phase ϕ_9, in agreement with the flow pattern evolution shown in Fig. 6.

C. *Strouhal Number*

The vortex shedding frequencies obtained from frequency spectra such as shown in Fig. 7 can be used to calculate the Strouhal number. Here the Strouhal number is based on the plate thickness, d, and the velocity amplitude at the entrance to the stack, u_M:

$$St_d = fd / u_M, \qquad (2)$$

where f is vortex shedding frequency.

The relationship between the Strouhal number and Reynolds number is plotted in Fig. 8. The detailed geometrical and flow information of this figure is referred as Table I. This figure covers all of the flow cases studied (including the three typical flow cases discussed in previous sections). It gives an empirical relation between the Strouhal number and both the plate thickness and the Reynolds number. It is clear that the Strouhal number increases gradually with the increase in the Reynolds number, but seems to saturate at the level between 0.18 and 0.2.

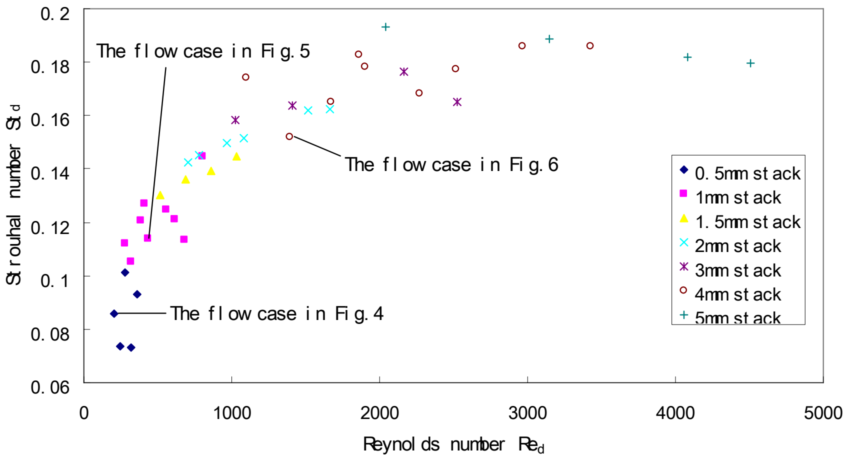

Fig. 8 Variations of Strouhal number with Reynolds number

IV. CONCLUSION

Particle Image Velocimetry was used to visualize vortex shedding processes at the end of parallel-plate stacks in the oscillatory flow. Standard hot-wire anemometry is also used to investigate velocity fluctuations in the acoustic cycle, in a selected location behind the plate, and estimate the Strouhal number related to vortex shedding processes. These two measurement results are compared with one another to understand the nature of vortex shedding in the cases studied. Some interesting results are found as follows:

1) With the variation of Reynolds number, different flow patterns of vortex shedding are visualized using the PIV technique. These different flow patterns are also represented by the hot-wire signal traces taken within an acoustic cycle, which can be used to derive characteristic Strouhal numbers. It is shown that there is a trend in the relation between the Strouhal number and the Reynolds

number, namely that St changes from about 0.07 to 0.2, but then saturates at a value close to 0.2

2) PIV results in Figs. 4-6 visualize two vortex shedding patterns. The first one is related to an instability of the elongated vortex structures, which leads to break-up into "vortex street" pattern as shown in Fig. 4. The second one shown in Fig. 6 seems to be related to the classical von Karman "vortex street", which is often found in the vortex shedding around the bluff body in steady flows. The vortex shedding pattern in Fig. 5 seems to be an intermediate mode between the two vortex shedding patterns. It is because in Fig. 4b (ϕ_4) the elongated vortex structure also breaks up into a "vortex street", and Fig. 4e (ϕ_8) shows alternate vortex shedding pattern as well. More interestingly, the Strouhal numbers show a gradual variation between the two extremes (the elongated shear layer break-up mode and the clear alternate vortex shedding mode) as shown in Fig. 8.

ACKNOWLEDGMENT

The authors would like to acknowledge the support received from the Engineering and Physical Sciences Research Council (EPSRC), UK and Universities UK.

REFERENCES

[1] Y. J. Chung and S. H, Kang, "A study on the vortex shedding and lock-on behind a square cylinder in an oscillatory incoming flow," *JSME International Journal, Series B*, vol. 46, no 2, pp. 250–261, 2003.

[2] C. Barbi, D. P. Favier, C. A. Maresca, and D. P. Telionis, "Vortex shedding and lock-on of a circular cylinder in oscillatory flow," *Journal of Fluid Mechanics*, vol. 170, pp. 527-544, 1986.

[3] M. Tatsuno and P. W. Bearman, "A visual study of the flow around an oscillating circular cylinder at low Keulegan-Carpenter numbers and low Stokes numbers," *Journal of Fluid Mechanics*, vol. 211, pp. 157-182, 1990.

[4] A. Okajima, T. Matsumoto, and S. Kimura, "Force measurements and flow visualization of bluff bodies in oscillatory flow," *Journal of Wind Engineering and Industrial Aerodynamics*, vol. 69-71, pp. 213-228, 1997.

[5] G.W. Swift, "Thermoacoustic engines," *The Journal of the Acoustical Society of America*, vol. 84, no. 4: pp.1145-1180, Oct. 1988.

[6] G.W. Swift, *Thermoacoustics: A Unifying Perspective for Some Engines and Refrigerators*. New York: Acoustical Society of America, 2002, ch. 4.

[7] P. Blanc-Benon, E. Besnoin, and O. Knio "Experimental and computational visualization of the flow field in a thermoacoustic stack," *C.R. Mecanique,* vol. 331, pp. 17 – 24, 2003.

[8] X. Mao, Z. Yu, and A. J. Jaworski, "PIV studies of coherent structures generated at the end of a stack of parallel plates in a standing wave acoustic field," *Experiments in Fluid,* vol. 45, no. 5, pp. 833-846, Nov. 2008.

[9] A. Berson, M. Michard, and P. Blanc-Benon, "Measurement of acoustic velocity in the stack of a thermoacoustic refrigerator using particle image velocimetry," *Heat and Mass Transfer,* vol. 44, no. 8, pp. 1015-1023, 2007.

[10] M. Hino, M. Sawamoto, and S Takasu, "Experiments on transition to turbulence in an oscillatory pipe flow," *Journal of Fluid Mechanics*, vol. 75, part 2, pp. 193-207, 1975.